Eidgenössische Technische Hochschule Zürich
Swiss Federal Institute of Technology Zurich

SED
Schweizerischer Erdbebendienst
Swiss Seismological Service

Report on site characterization

Böbikon, Switzerland (BOBI)

Poggi Valerio, Donat Fäh

Last modified - 22 / 12 / 2014

1. Introduction

In the framework of the NAGRA seismic network project, an array measurement of the ambient vibration wave-field was performed at the location of the SED borehole station BOBI (Böbikon, Switzerland). The scope of the survey is the seismic characterization of the area surrounding the installation (**Figure 1**), which consists in a short period borehole sensor at about 100m, and a collocated strong motion seismometer at the surface, with a high-resolution digitizer (Taurus 24Bit @200sps). Ambient vibration analysis has been used to infer the characteristics of the underground structure of the site, with special regard to the one-dimensional shear-wave velocity. Such profile was later compared with the results from active seismic measurements and used to assess the local seismic response of the station.

For the analysis, different spectral analysis techniques were implemented, consisting in both single and array methods, which are listed below:

- Time-frequency wavelet analysis
- Power-spectral density estimation
- Conventional horizontal to vertical spectral ratios
- Directional horizontal to vertical spectral ratios
- Wavelet polarization analysis
- Three-component high-resolution f-k analysis.

The results of all these analyses conformed to the definition of the final velocity model. In the following, the main results of these investigations are summarized and a final interpretation of the velocity profile is given. From this interpretation, engineering parameters are finally derived, e.g. the Qwl-Vs average velocity, VsZ (including Vs30) and the seismic amplification from the analytical SH-transfer function of the one-dimensional soil column.

2. Survey description

To characterize the seismic response of the site, an array measurement of ambient vibration was performed on 19/03/2014 (**Figure 1**). The array consists of two measuring configurations (A1 and A2) of 14 sensors each and increasing diameter of about 120m and 300m respectively. The two configurations were planned to partially overlap, by sharing 9 common sensors, with the aim of providing a continuous frequency resolution between the two geometries. Second configuration was initially planned to be smaller, but unforeseen circumstances (a farmed field) forced the geometry to cross the nearby forest. Configuration A1 recorded for a total of 1h30m, while configuration A2 for 1h only. As a general rule, larger arrays would require longer recording time to produce a reasonable statistics of the ambient vibration processing results. In this case, however, due to the difficulties in the setup of the second configuration, the available time for recording was limited. Satisfactory results were nevertheless obtained. For the larger configuration, a penetration depth of about 200~250m was initially expected.

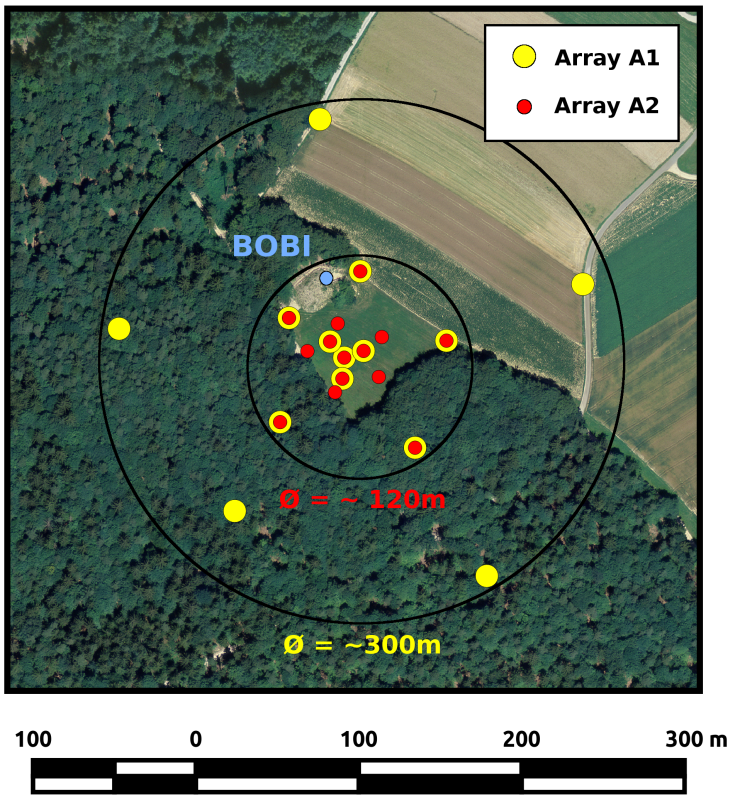

Figure 1 - *Location of the ambient vibration array survey performed in Böbikon, (SED station BOBI) on 19/03/2014. Two concentric configurations of increasing diameter were implemented (named A1 and A2). Location of the permanent station is shown in blue.*

3. Soil type, topography and geology

The array has been set in open field conditions, in a rural area (**Figure 1**, **Figure 3**). The influence of buildings and anthropogenic disturbances is virtually negligible. However, recordings have been affected by harmonic contributions (see section 6) in relatively narrow frequency bands. Array sensors have been deployed on free soil. Good coupling with the ground was assured by means of digging small holes at the sensor's places, and by using a special support (*Trihedron*®) that facilitates the leveling of the device even for difficult soil conditions. The measurement area was located on a nearly flat area; therefore no topographic correction was necessary before processing.

4. Weather conditions

The weather conditions were optimal and stable during the whole measurement, with no precipitations, no wind and an average temperature of 15 degrees.

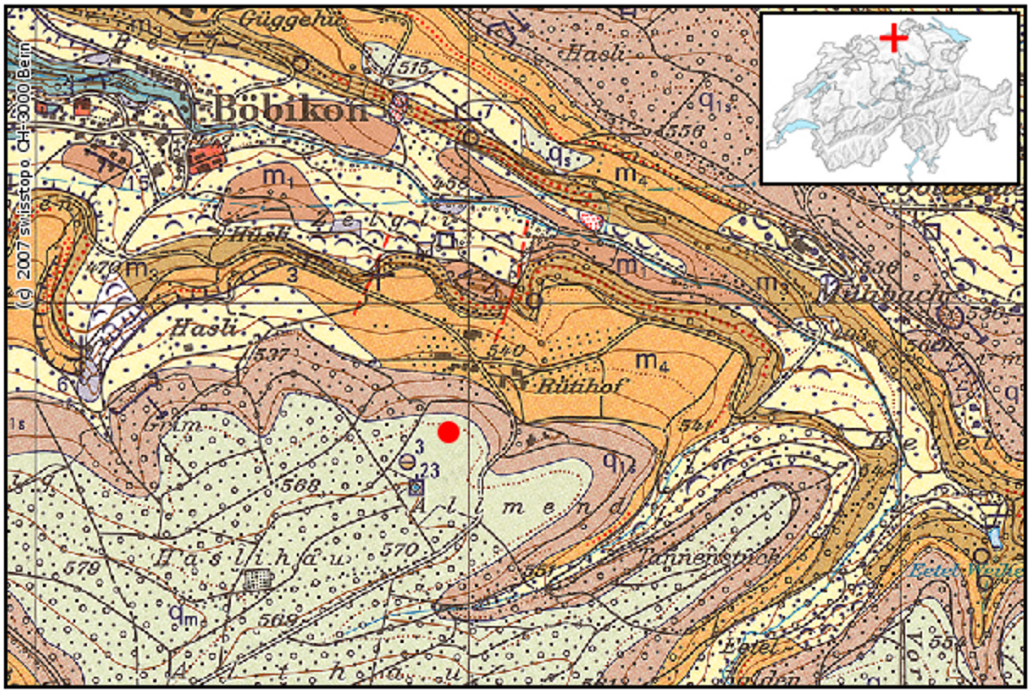

Figure 2 - *Geological map of the measuring area, in the surroundings of Böbikon (reproduced from Swisstopo, "Geologische Generalkarte der Schweiz", modified). In red the approximate location of the permanent station BOBI.*

From the geological points of view (**Figure 2**) the target area is located on the western edge of the Tabular Jura. The surface morphology is considerably smooth and modeled by the action of glaciers during the Pleistocene. The station is likely located on top of a large moranic deposit, clearly identifiable from the surface morphology and confirmed by the geological map of the area (unit Q_m and Q_{1s}). Geophysical bedrock is never exposed (supposedly deep at the measuring location) and is likely composed of consolidated sandstones and conglomerates of the Molassic basin (unit m_4) of Miocenic age. A variable-thick cover of quaternary soil material is generally present. Such site can be classified as of rock ground-type A.

5. Acquisition equipment

Each acquisition point within the array consisted of a three components seismometer (Lennartz 3C with 5s eigenperiod) and a 24 bit data logger (Quanterra Q330). Synchronization between stations was assured by standard GPS, while a more accurate differential GPS (Leica Viva system) was used to precisely locate the sensor's coordinates with a tolerance of less than 5cm.

Figure 3 - *Overview of the measurement area. Location of the SED station BOBI is indicated by the red arrow.*

6. Pre-processing and preliminary data-quality control

The three-component recording has been filtered prior to analysis using a band-pass 6th order causal Butterworth filter with corners at 0.2Hz and 50Hz. Although it is not a strict requirement for spectral analysis techniques, such filtering was applied in order to facilitate the preliminary visual inspection of the noise traces and to evaluate the coherency of the wave-field (**Figure 4**). Such procedure gives essential information for the subsequent interpretation of the f-k analysis results.

Contrary to expectation (given the rural location), the recordings have been affected by a certain amount of high-frequency transients. Additionally, two stations did not properly work; station BOB10 had a cable failure, while station BOB08 did not register the N-S component for unknown reasons (**Figure 4**). These stations were discarded from the analysis. To assess the quality of the ambient vibration recordings, spectral analysis was subsequently performed. Because of the stochastic nature of the ambient vibration wave-field, a statistical approach has to be used, such as the estimation of the power spectral density (*PSD*). This approach is useful to evaluate the average energy level of the recordings in the analyzed frequency range, and to access the presence of spurious spectral peaks, which might be related to human activity (machinery, pumps).

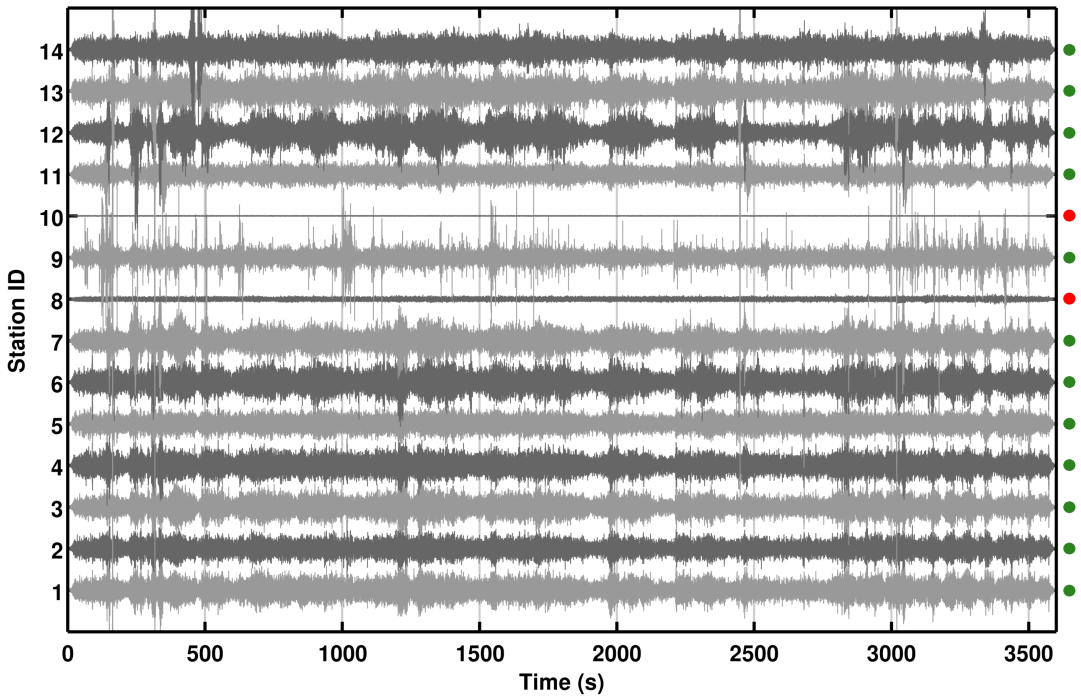

Figure 4 - *Inspection of the useful part of the ambient vibration recording of the Böbikon array (here configuration A2). A certain amount of short high-frequency transients were present during the acquisition, which nevertheless did not bias the subsequent f-k processing results.*

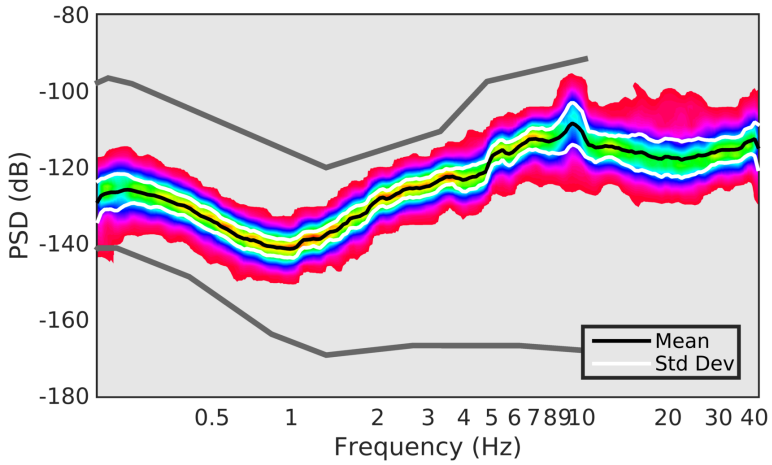

Figure 5 - *Power spectral density (PSD) computed for 1h30m recording at the central station of the array configuration A2, horizontal direction N-S. Similar results were obtained for the other stations of the array. In gray lines are the minimum and the maximum bounds of the USGS noise model, for comparison.*

By inspecting the PSD of all the three-component recordings of the array in the range between 0.5 and 40Hz, is found that the average energy level of the spectrum is overall very low at low frequencies (roughly < 1Hz), while it tends to progressively increase at increasing frequencies, nevertheless well within the minimum and maximum bounds of the USGS noise model (**Figure 5**) Two peaks of possibly anthropogenic origin are clearly visible, at about 5 and 9 Hz. These bands should be properly rejected from interpretation and processing.

Complementary to the aforementioned statistical methods, a spectral decomposition approach is more suitable to assess the stationarity of the ambient vibration wave-field over time. The wavelet time-frequency analysis was then performed over the whole recording time. From such analysis (**Figure 6**) an overall stability of the ambient-vibration wave-field over time is evident. The two disturbances at about 5Hz and 9Hz are confirmed to be nearly harmonic contributions, steady over the whole recording window. This provides a further confirmation of their possible anthropogenic origin. A strong additional harmonic signal is evident, at 6.5Hz, but not always present on the recordings. All these disturbances are nevertheless well localized in frequency; therefore they won't likely affect the following processing steps.

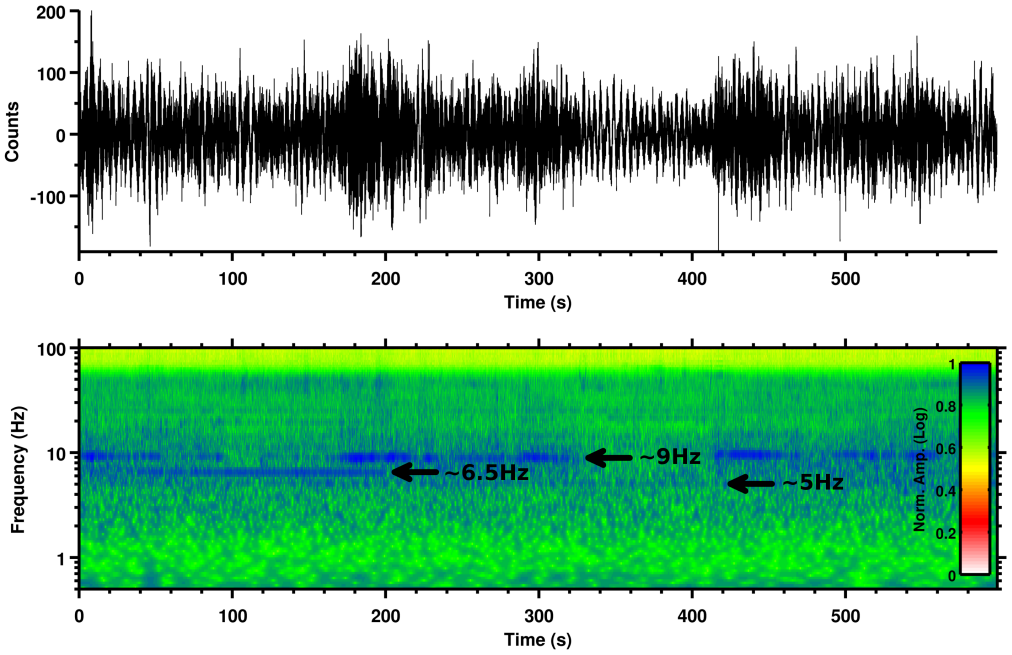

Figure 6 - *Example of spectrogram from 600s of recording of the central station (BOB01) of the array configuration A2. Harmonic disturbances are visible on the whole spectrogram, at about 5Hz, 6.5Hz and 9Hz. These signals were also present during the recordings of configuration A1. For the analysis, the cosine wavelet is used (wavelet parameter = 12).*

7. Conventional H/V spectral ratios

The horizontal-to-vertical (H/V) Fourier spectral ratio is a technique widely used in seismic site characterization because of its ability to provide an estimate of the SH wave fundamental frequency of resonance (f_0) of the site. Other than that, H/V ratios are useful to provide information on the Rayleigh wave ellipticity function, which can be used in surface wave dispersion inversion procedures to constrain large velocity contrasts at depth. In this study, we use the H/V technique also to map the variability of the subsoil structure along the investigated area; this is necessary to verify the fulfillment of the 1D structure assumption, which is necessary for the f-k method applied later.

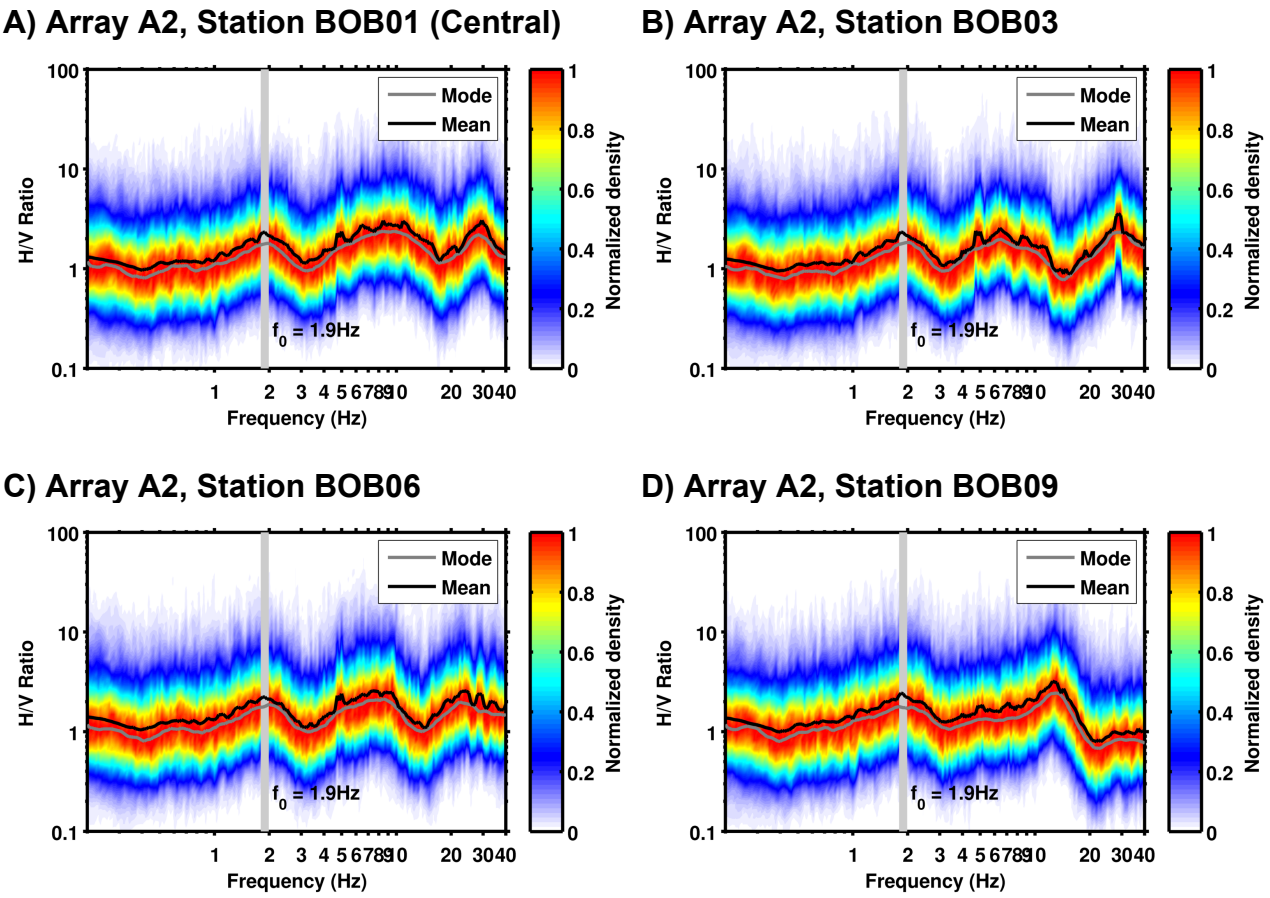

Figure 7 - *Example of H/V spectral ratios for the configurations A2. The resonance frequency of the soil cover is indicated with a light gray line (~1.9Hz). An additional peak is visible in a range between 7 to 15Hz. A third peak is also occasionally visible at rather high frequencies.*

H/V spectral ratios have been computed for all the recordings at each station of the array and separately for configurations A1 and A2 (e.g. **Figure 7**). The behavior of the noise wave-field at the different stations location is comparable at low frequencies (roughly < 9Hz), while the high frequency region shows more variability, within and between arrays. In average (**Figure 8**) spectral curves show a relatively stable low frequency peak (around 1.8~1.9Hz). Such maximum is likely induced by a change in lithology at depth, which causes a modest contrast of seismic impedance. The peak should be regarded as the fundamental resonance frequency of the site (f_0). A second broad peak is also present between about 7Hz and 10Hz, stable on nearly all stations. Interpretation of this second peak is however not straightforward; it might be related to a secondary velocity interface at intermediate depth or – more likely - to the some maximum in the Rayleigh ellipticity function. This will be clarified after the inversion phase. A third peak is finally also present at very high frequency in most (but not all) of the stations. Such maximum is of more difficult interpretation; but probably induced by the Quaternary soil cover, which can be very heterogeneous over the measuring area. The behavior of the site can be considered laterally homogeneous for the f-k analysis.

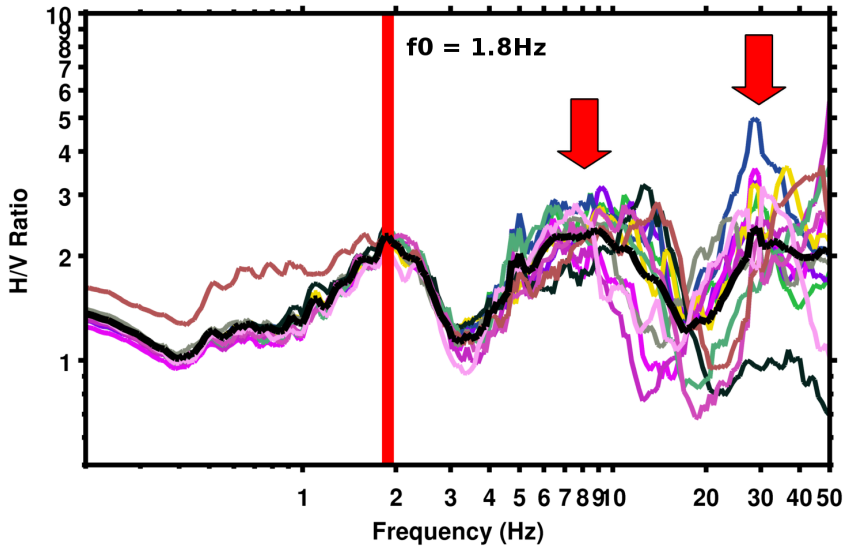

Figure 8 - *Comparison of the H/V spectral ratio curves of all the stations of the array (in this example for the array configuration A2). The curves are stable up to at least 10Hz, confirming the lateral homogeneity of the underlying bedrock velocity structure of the site. A low frequency peak (f_0) is visible at about 1.8~1.9Hz. Two additional peaks can be identified at 7-10Hz and ~30Hz.*

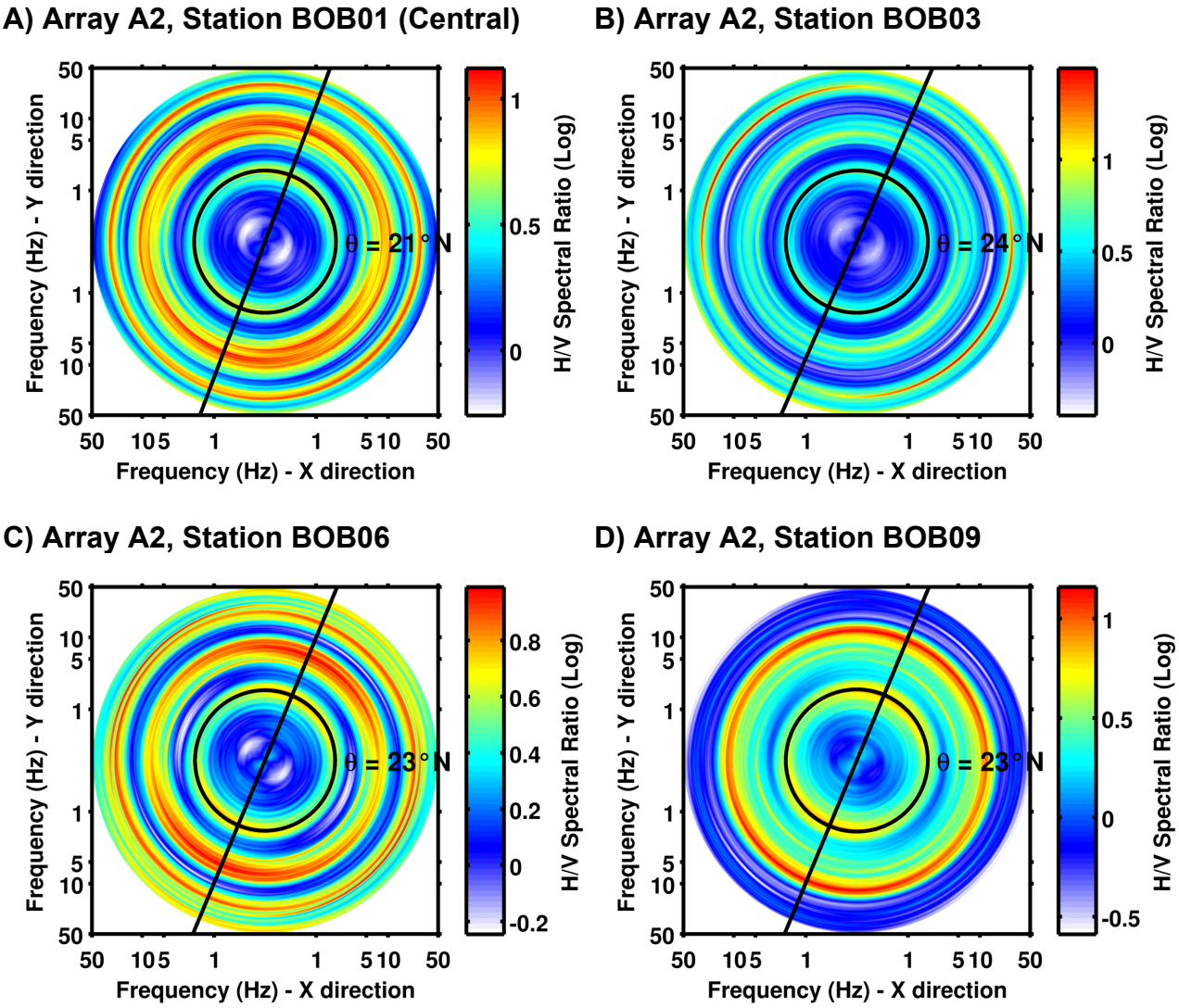

Figure 9 - *Example of directional H/V spectral ratios for configuration A2. The low frequency resonance peak (f_0) is preferentially and consistently aligned roughly NW-SE (~22-23°). No common pattern can be defined for the second and the third peak.*

8. Directional analysis

The computation of directional H/V spectral ratio or polarization analysis is useful to reveal asymmetries in the ambient vibration wave-field. Different effects can induce such a behavior: 2D/3D structure, topographic effects or a non-homogeneous distribution of the noise sources. If a strong directionality is found by the analysis, it is generally recommended to carry out further investigations to properly address the origin of polarization. By processing the directional H/V ratios at all the recording stations of the array (e.g. **Figure 9**) it is possible to describe some directionality in the ground motion. The fundamental frequency shows a preferential (very stable) alignment along direction NW-SE, roughly 22~23°, visible on most of stations of the two geometries. Such direction has however no direct relation with none of the topographic features of the area, and might be therefore induced by some preferential distribution of noise source or to some irregularity of the bedrock geometry at depth (dipping?). Second option seems to be more plausible, since noise source directionality would also (partially) affected the higher frequencies. No preferential direction pattern can be observed for the second or the third peak.

The results of the H/V directional analysis are partially confirmed by applying the wavelet polarization analysis technique (Burjanek et al., 2008). Here, the particle motion shows to be mostly elliptical, with just a weak polarization at the resonance frequencies (**Figure 10**). The second peak is also weakly polarized, which supports its relation to ground structure. A very weak directionality on azimuth is visible at f_0 (**Figure 11**A), nevertheless consistent with H/V results.

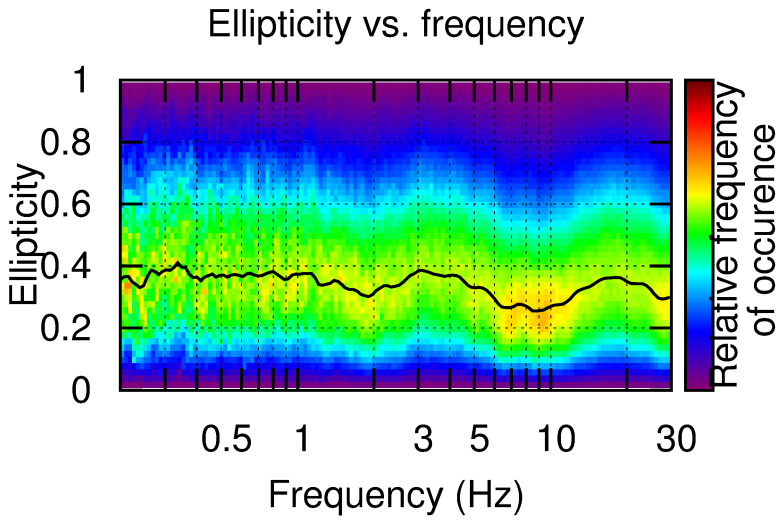

Figure 10 - *Ellipticity of the particle motion from wavelet-based polarization analysis at the central station of the array (BOB01). Similar results can be obtained for other stations of the arrays.*

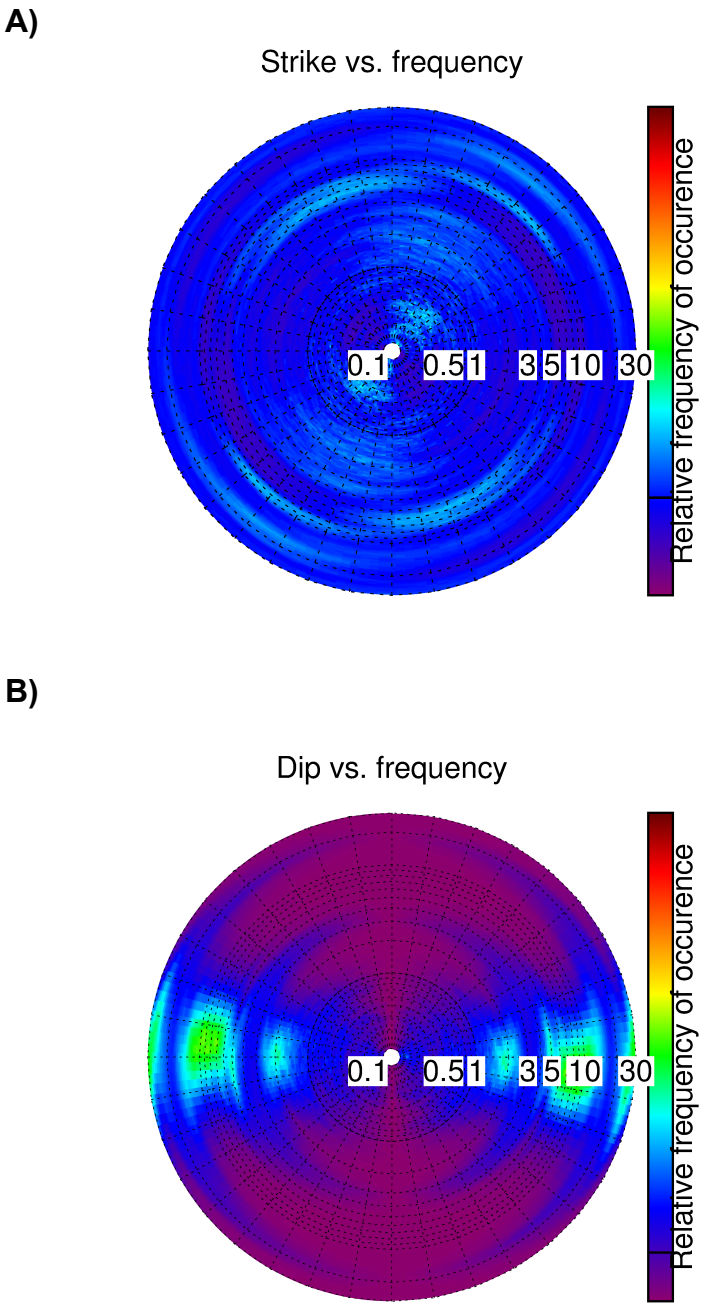

Figure 11 - *Directionality of the particle motion from wavelet-based polarization analysis (dip direction in A, strike in B) at the central station of the array (BOB01). Similar results can be obtained for other stations of the arrays.*

9. Three-component f-k analysis

The frequency-wavenumber analysis is a spectral technique based on seismic array recordings that allows retrieving direction and dispersion characteristics of the surface waves. We apply this technique to three-component ambient vibration recordings using a modification of the high-resolution method of Capon (1969) as described in Poggi et al. (2010). Using all the three-components of motion gives the possibility to retrieve information about the propagation of the Rayleigh waves (vertical and radial processing direction) as well as of the Love waves (transversal direction).

As in the case of the previous methods, the ambient vibration recordings are treated statistically by subdividing the traces in sub-windows. For each consecutive window a separated f-k analysis is performed, and the results are then averaged over the whole recording, increasing the robustness of the final estimation.

A) Ring 2, 3-5Hz

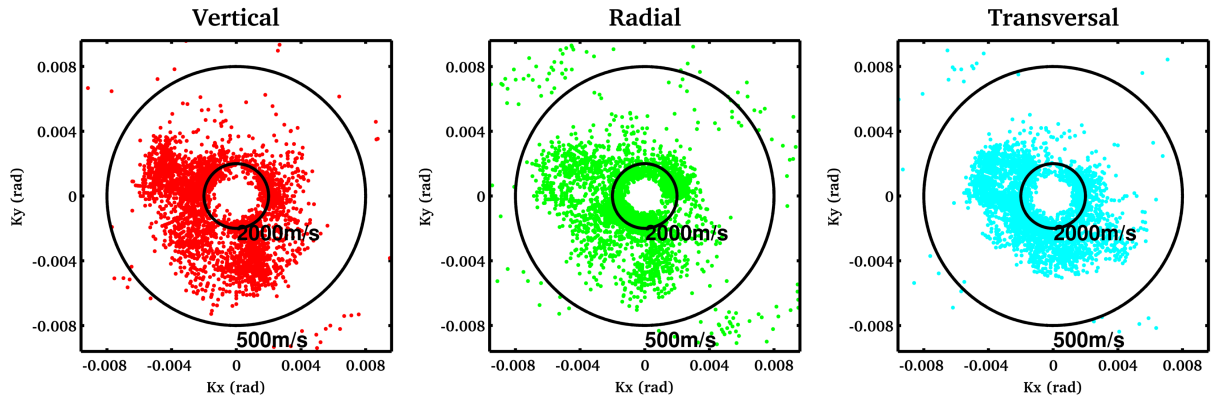

B) Ring2, 5-10Hz

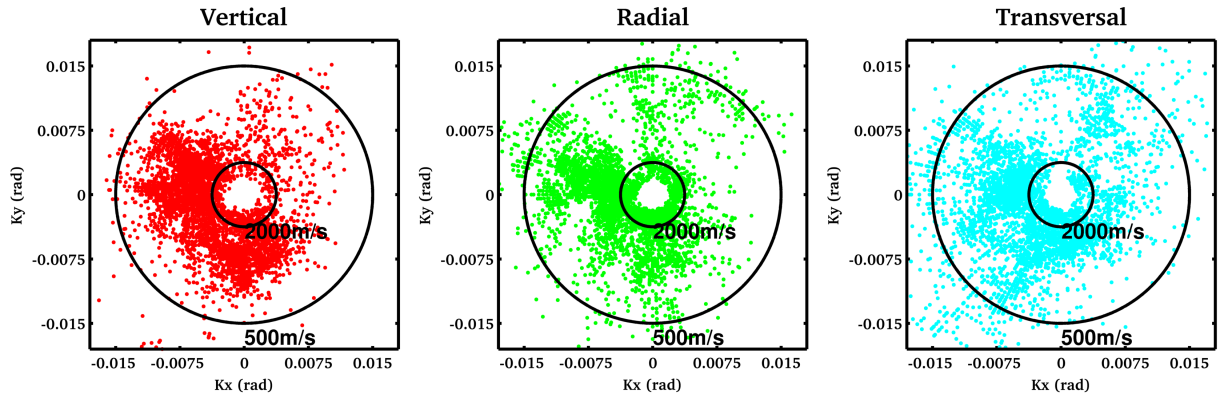

Figure 12 - *Example of distribution of noise sources in the low (3-5Hz) and intermediate frequency range (5-10Hz) obtained from three-component f-k analysis. The source distribution is irregular but not strictly directional on all the propagation components.*

As first step, from the f-k analysis it is possible to assess the azimuthal distribution of noise sources over different frequency ranges (e.g. **Figure 12**) separately for the vertical, the radial and the transversal direction of polarization. From the analysis of the two geometries A1 and A2, source distribution appears to be slight inhomogeneous in all the components, with a preferential clustering of sources in the SW quadrant.

As a second step, the surface-wave dispersion curves are extracted by visual inspection and manual picking of the f-k density plots (**Figure 13** and **Figure 14**), separately for the three polarization directions. Complementary results have been obtained for the three array configurations. In particular, Love wave's fundamental mode dispersion can be well tracked in a broad frequency range (from 2.5Hz to about 30Hz) on both A1 to A2; velocity estimates are also consistent and well overlapping between the two geometries. Rayleigh wave's fundamental mode can be well tracked from about 3Hz to 10Hz on the vertical direction and for both array configurations, while radial direction provides reliable results only for configuration A2. A second higher mode is occasionally visible, but well consistent between vertical and radial directions and between configurations.

A summary of all the identified modes from vertical, radial and transversal direction of propagation is presented in **Figure 15**, while the final interpretation of Rayleigh and Love wave dispersion pattern is in **Figure 16**, together with the results from an active seismic survey performed on the same location by the company *RoXplore*. Active surface wave analysis results (MASW) are compatible with our interpretation, extending the resolution at high frequencies and adding a Rayleigh wave higher mode to the interpretation model.

10. Inversion of the dispersion curves

The surface wave dispersion curves (Rayleigh and Love) obtained from the three-component f-k analysis of the ambient vibrations and the fundamental frequency of resonance (f_0) from average H/V spectral ratios are inverted to obtain an estimation of the velocity profile of the site (mainly S-wave velocity as function of depth, and to a lesser extend the P-wave velocity, due to the lower sensitivity). The analysis is performed using the software *Dinver* (www.geopsy.org), which implements a direct search approach (**Figure 17**) based on a conditional version of the neighborhood algorithm (Sambridge, 1999).

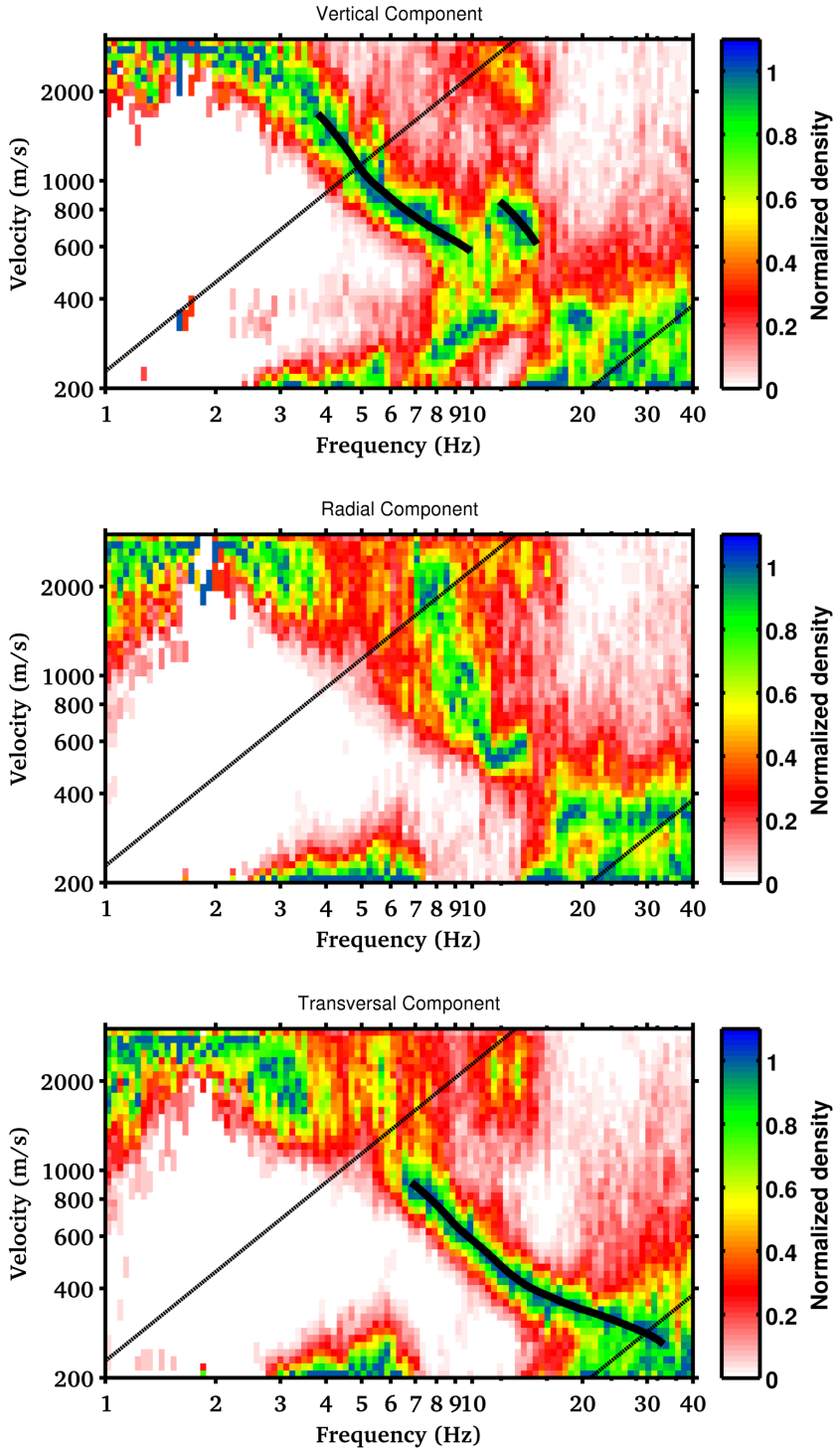

Figure 13 - *Density distribution of the surface wave signals obtained from the recording of the array configuration A1 using three-component f-k analysis. From top to bottom: Rayleigh vertical, Rayleigh radial and Love wave dispersion. In red the interpreted dispersion curves are given (manually selected).*

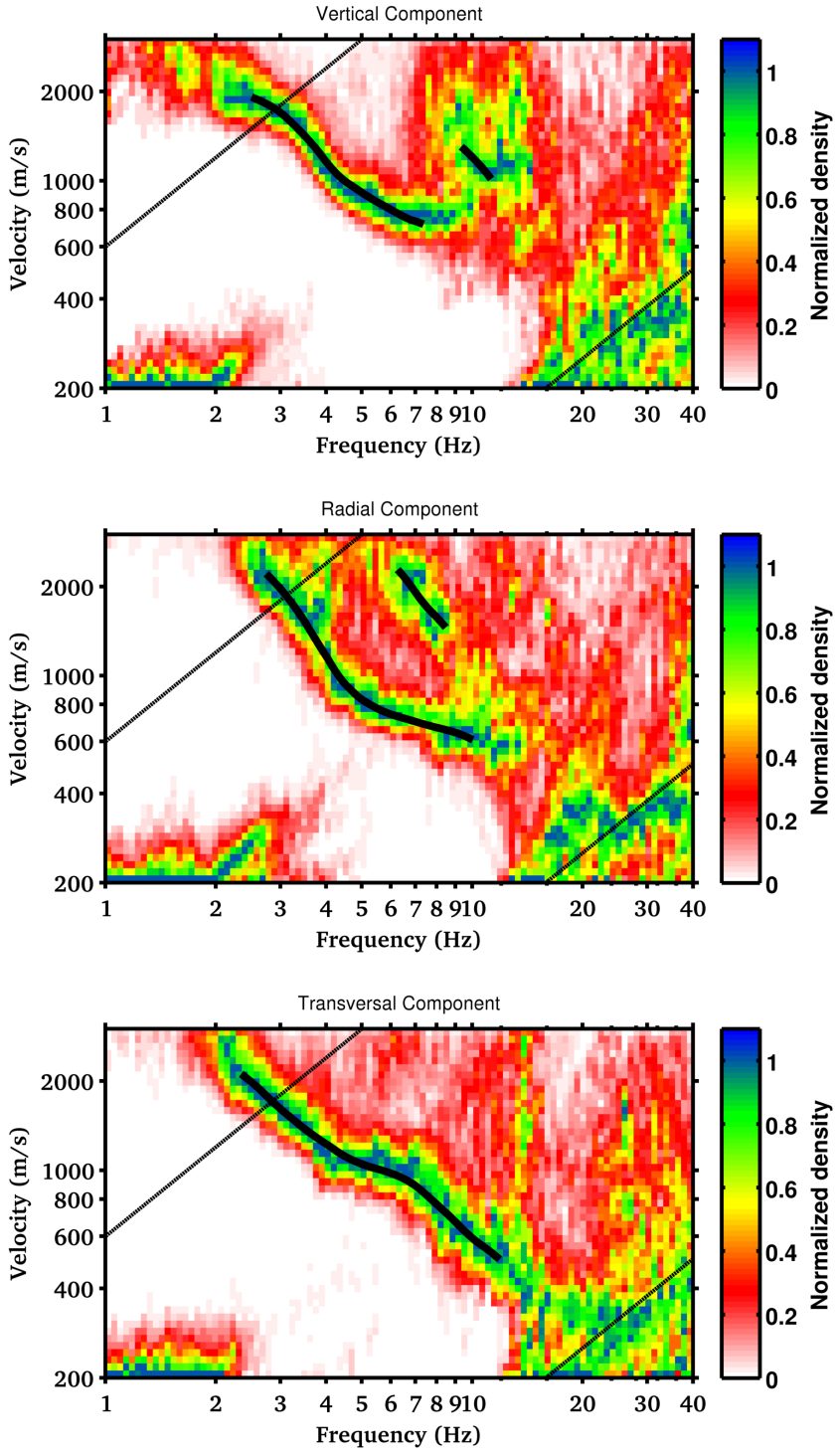

Figure 14 - *Density distribution of the surface wave signals obtained from the recording of the array configuration A2 using three-component f-k analysis. From top to bottom: Rayleigh vertical, Rayleigh radial and Love wave dispersion. In red the interpreted dispersion curves are given (manually selected).*

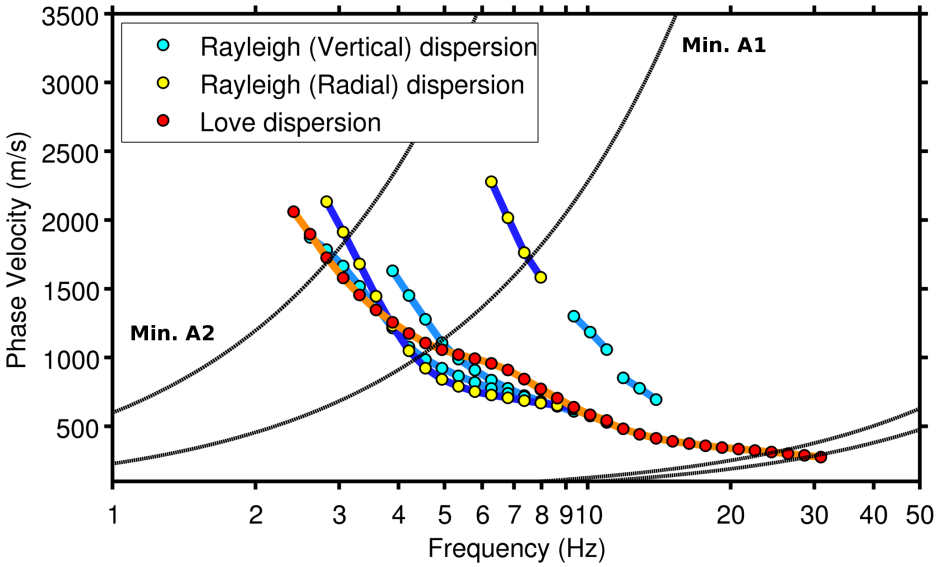

Figure 15 - *Summary of all dispersion curves obtained from three-component f-k analysis of the three array configurations A1 and A2. Minimum and maximum resolution bounds from the two geometries are indicated with black solid lines.*

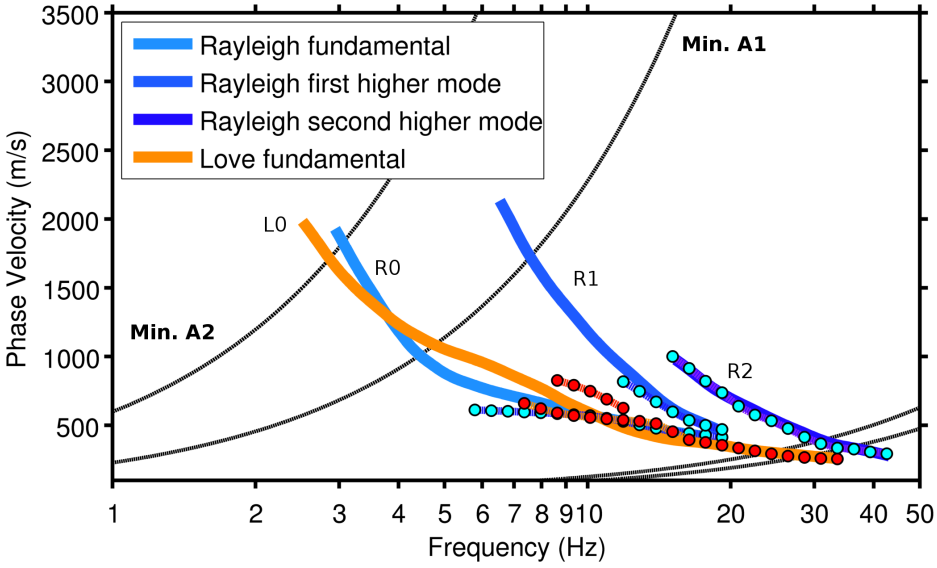

Figure 16 - *Final interpretation of the Rayleigh and Love dispersion curves for BOBI, including the results from active surface wave analysis (MASW, with dots). Minimum and maximum resolution bounds from the full array are indicated with black solid lines.*

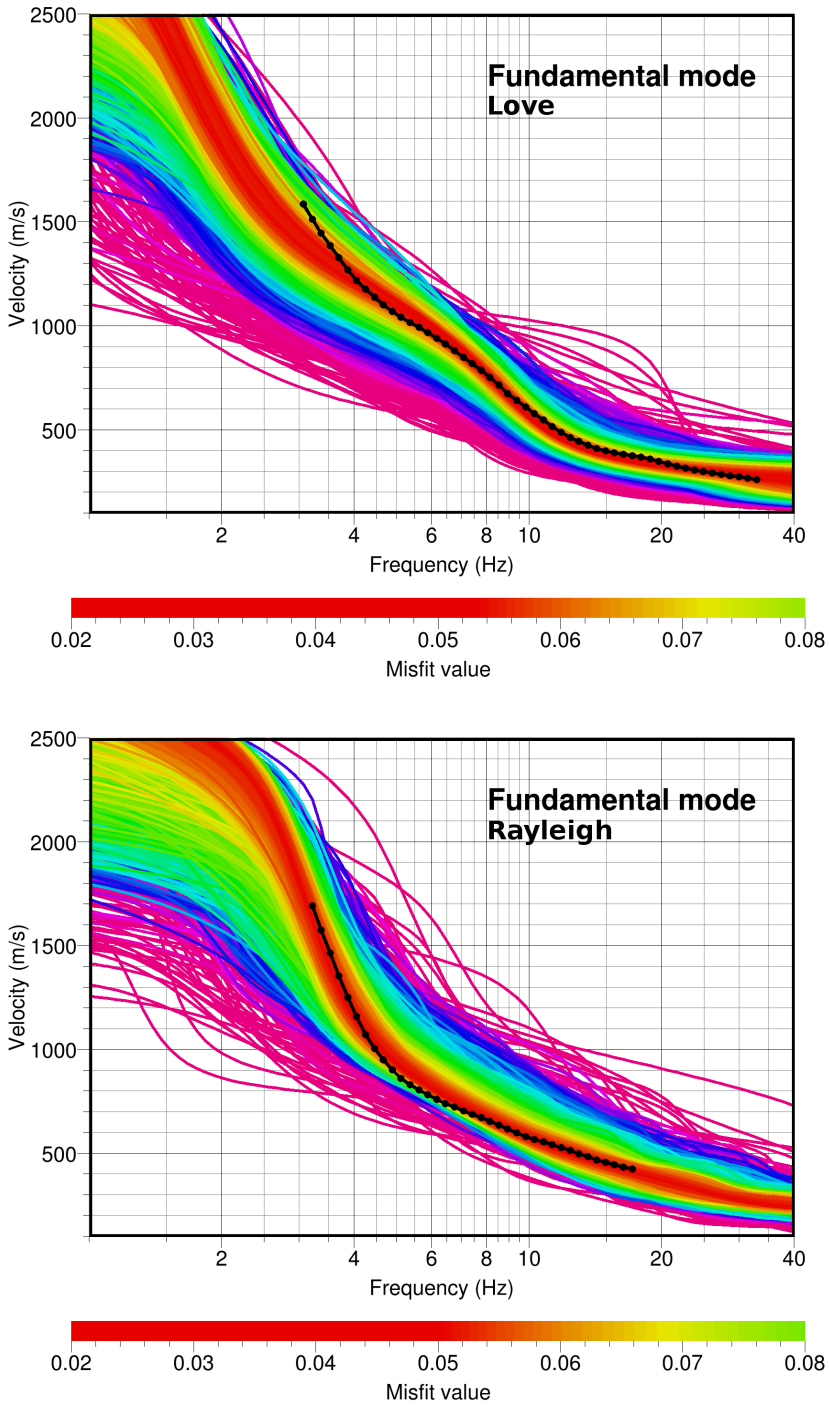

Figure 17 - *Example of fitting the surface dispersion data within the global optimization procedure. Different colors represent different misfit between the observed (in black) and the modeled dispersion curves during the search.*

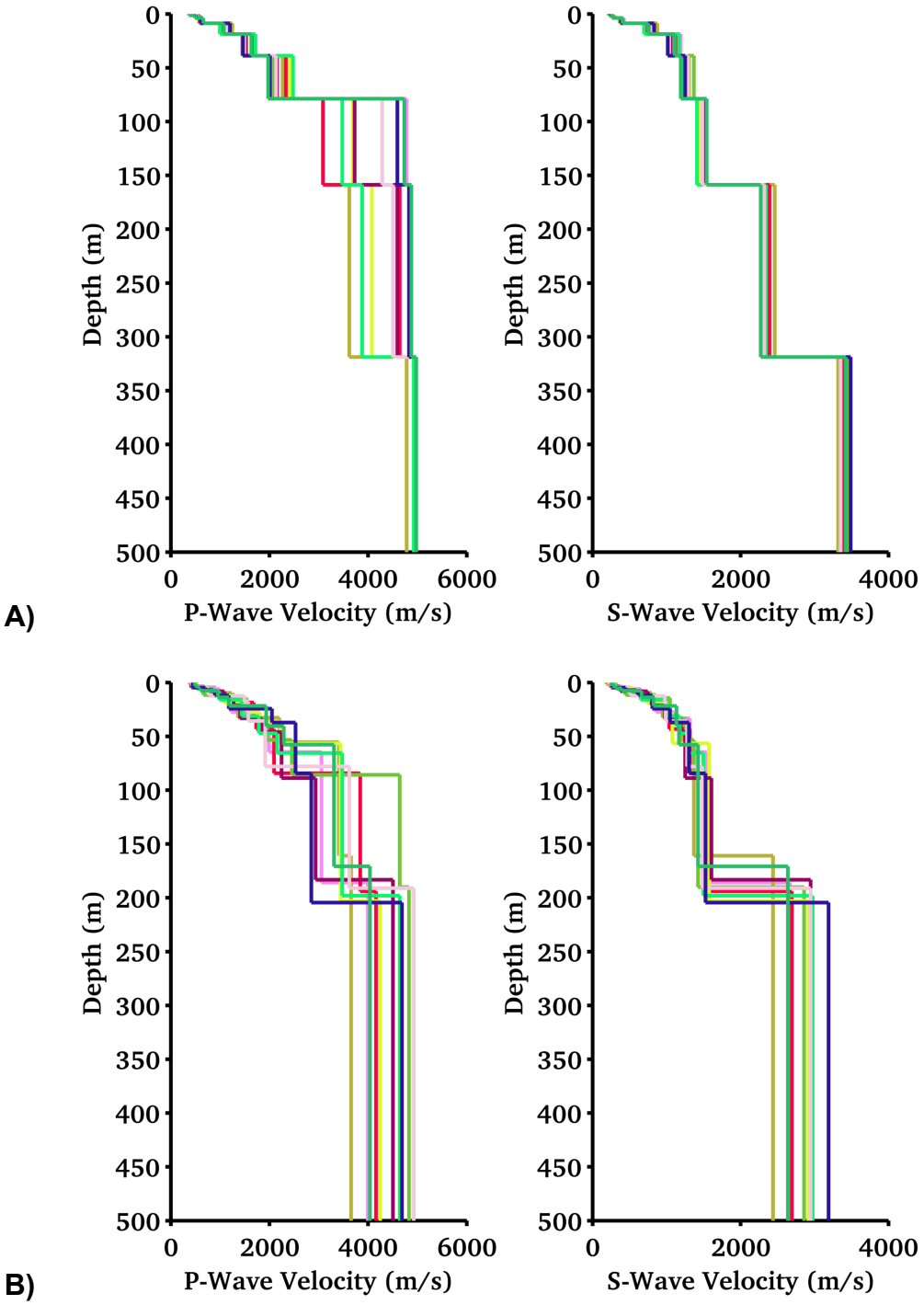

Figure 18 - *Collecting the best fitting models from the ten separated inversion runs using the free-layers (A, top) and fixed-layers (B, bottom) parameterization schemes.*

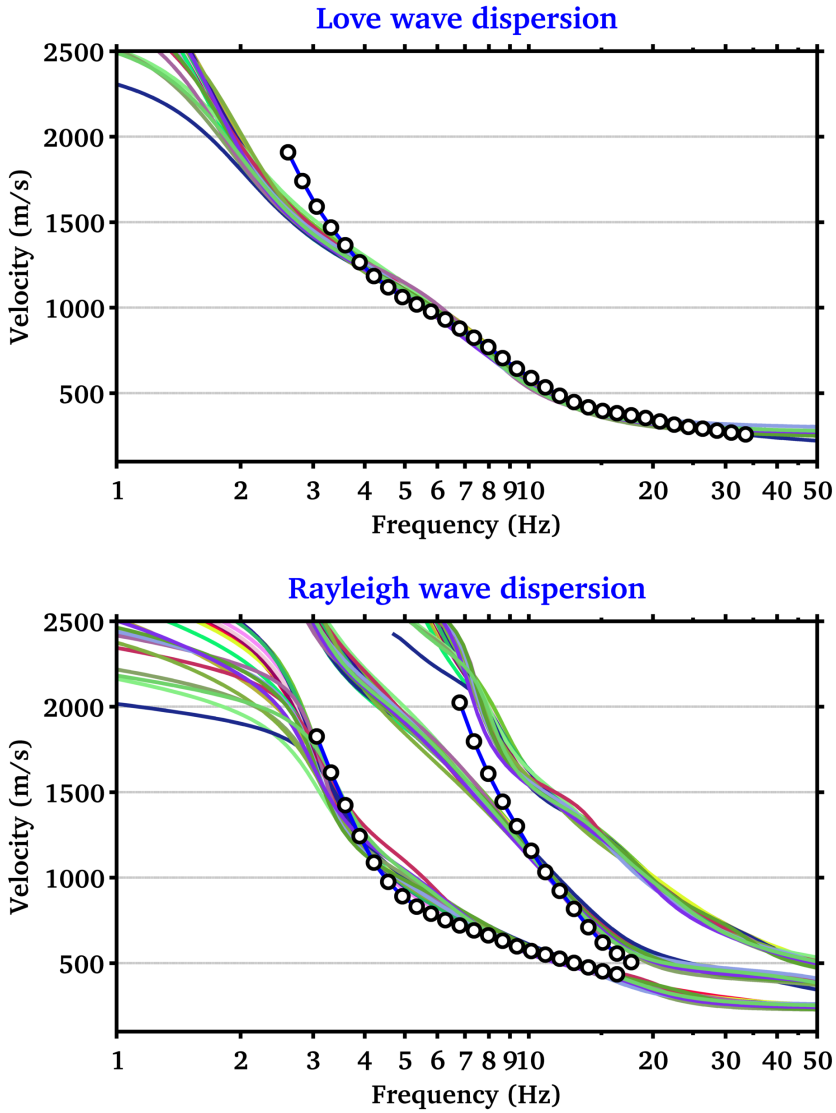

Figure 19 - *Dispersion curves computed from the best fitting models of the two proposed interpretation schemes (free and fix layers), compared with picked dispersion from active and passive seismic experiments.*

To parameterize the velocity model, two different approaches were implemented. The first one consisted in setting up an eight-layer model with fix interface depths. In such a case the free inversion parameters are then the velocities (P and S) and layer thicknesses. In the second case, a free-thickness layer approach was used. The advantage of the former method stays in the possibility to better resolve sharp velocity interfaces, while the second is less unique and better constraints the seismic velocity. The two approaches have to be nevertheless considered complementary, and they should provide consistent results.

Ten inversion tests (*runs*) were performed for each of the two model schemes, in order to minimize the effect related to a possible unfavorable initial randomization of the parameter space. The best fitting model from of each run was then collected (**Figure 18** and **Figure 21**) and used later on for the computation of the derived soil parameters.

In more detail, the inverted velocity profiles (Vs and Vp) are gradient-like in the top part, with a major interface between about 150m and 250m. While top part is actually constrained by high frequency part of the Rayleigh and Love dispersion curves (including results from active surface wave analysis, **Figure 19**), the interface is solely controlled by the use of f_0 form H/V spectral ratios (**Figure 20**). By subsequent comparison, the theoretical ellipticity is nevertheless matching the shape of great part of the whole average H/V curve, including the second peak (which can then be addressed to Rayleigh wave), but not the third peak (then probably an effect of the soil cover).

By considering the minimum available frequency of the surface-wave analysis, and by analyzing the scattering of the inverted models (**Figure 21**), it is realistic to assume the velocity profiles to be reliable down to a depth of about 150~250m. Below this value no direct constrain is available from data, and the velocity values are obtained by pure extrapolation.

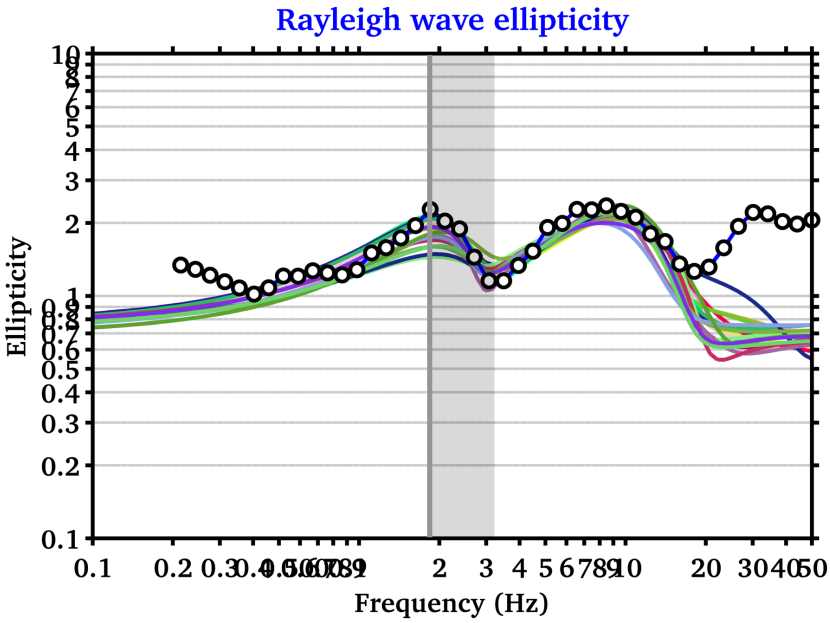

Figure 20 - *Rayleigh wave ellipticity curves computed from the best fitting models of the two proposed interpretation schemes (free and fixed layers), compared with average H/V spectral ratio from configuration A2 (scaled by sqrt(2)). The first two peaks are clearly reproducible, even though the whole H/V curve was not used during the inversion.*

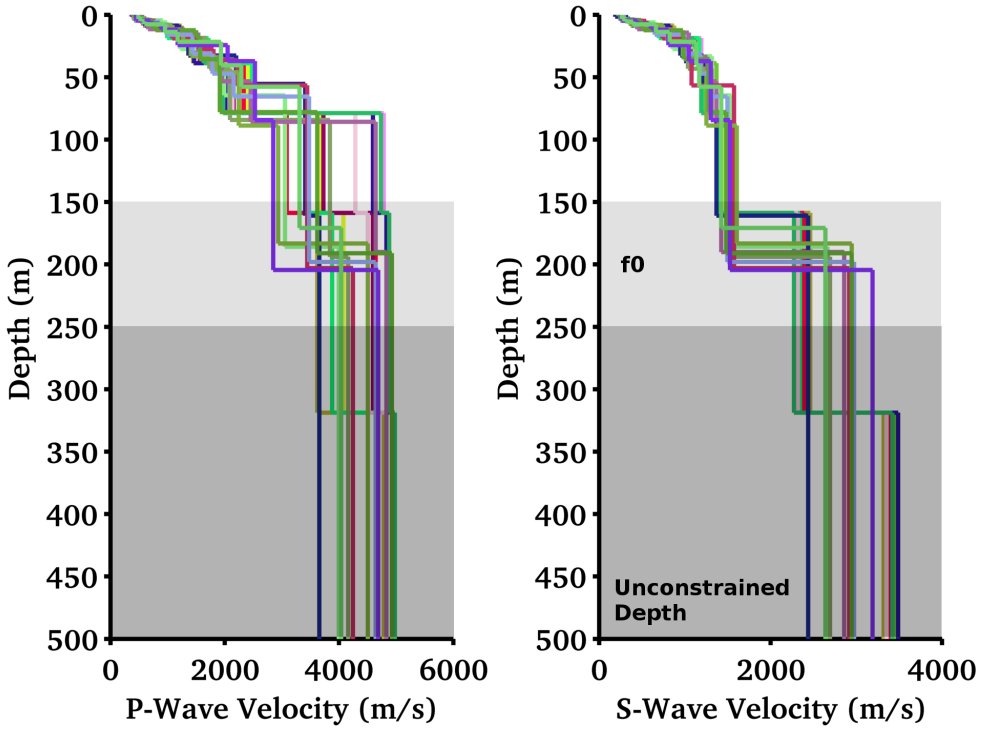

Figure 21 - *Comparison of all the best models from the two parameterization schemes (free and fixed layers). The two approaches produce consistent results. Depth range between about 150m and 250m is solely constrained by f_0 and should be considered approximately the maximum resolved depth.*

11. Engineering soil parameters

The ensemble of all the best inverted velocity profiles is then used to derive average soil parameters like the VsZ (average travel-time S-wave velocity over the depth Z, including Vs30, Table 1) and the quarter-wavelength (QWL) average velocities (Joyner et al., 1984) for a range of frequencies between 0.6 and 30Hz (**Figure 22**). The former is a standard parameter for the classification of ground-types in most building codes and in ground motion prediction equations. The latter is a parameter useful for the empirical estimation of the site-response and to assess the sensitivity of the seismic wave-field to the different depths. It has to be noticed that these two parameters are derived separately from all the best S-wave velocity models obtained from the inversion, and the results is finally averaged to improve statistics.

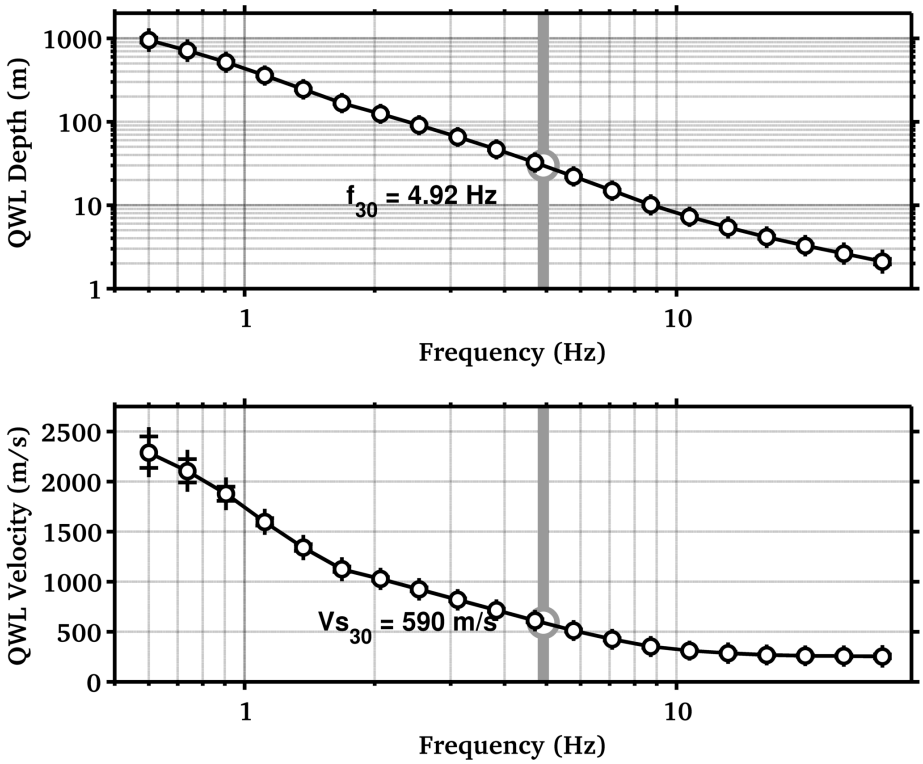

Figure 22 - *Quarter-wavelength representation of the inverted S-wave velocity profiles. Top: the depth-frequency dependency. Bottom: the QWL average velocity. The Vs30 value is indicated with its corresponding QWL frequency.*

12. Amplification models

Site amplification functions have been computed using two different approaches: the S-wave transfer function for vertical propagation and the quarter-wavelength amplification. In general the first method is used to evaluate the resonance characteristics of the site, while the second is more useful to assess the effect of the velocity contrasts between the lowermost rock layer (as reference) and the different QWL averaging depths. The two amplification functions are then corrected for the Swiss rock reference velocity profile as defined in Poggi et al. (2011), according to the procedure described in Edwards et al. (2013). Given the lower velocities in the uppermost part of the BOBI profile compared to the Swiss reference, the final corrected amplification function shows a lower average amplification level at high frequencies than the uncorrected (**Figure 23**).

Averaging depth (m)	Vs-mean (m/s)	St.Dev.
5	279.95	10.38
10	350.94	6.34
15	425.41	5.16
20	486.22	5.58
25	542.75	6.45
30	**590.02**	**7.46**
40	668.27	7.93
50	736.00	8.73
75	859.28	10.16
100	955.85	11.90
150	1084.30	15.41
200	1212.99	24.30

Table 1 - *Average travel-time velocities at different depths. Vs30 is highlighted.*

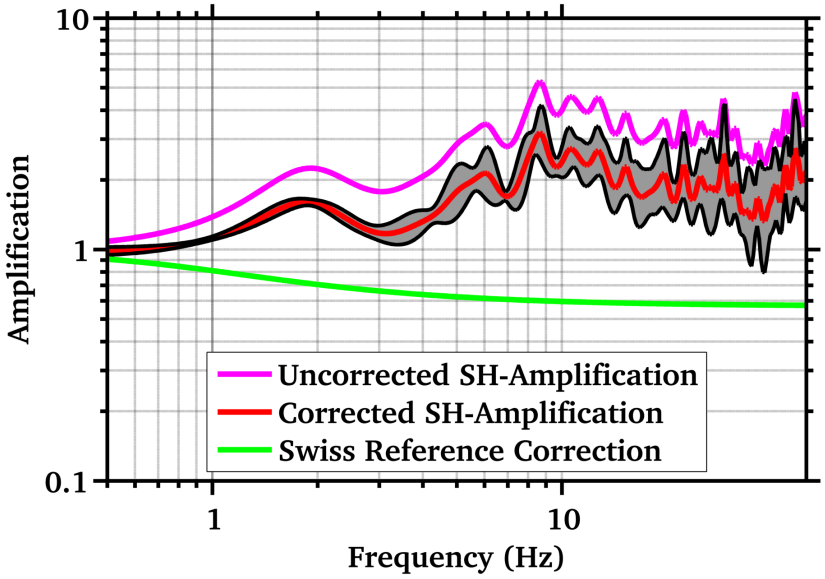

Figure 23 - *Correcting the SH-wave transfer function for the Swiss (rock) reference conditions (Poggi et al. 2011). The final corrected amplification function shows a lower (average) amplification at high frequencies than the uncorrected.*

Amplification functions using the transfer function and the quarter-wavelength approach are comparable (**Figure 24**), even if the transfer function provides a slightly larger amplification, because of the presence of some weak resonance peaks. At low frequencies both methods converge to the same amplification level. It has to be notice that the amplification functions do not include attenuation at this stage of the analysis, as the quality factors of the site are too uncertain.

A good matching is obtained by comparison between the one-dimensional transfer function and the empirical amplification from spectral modeling of low-magnitude earthquakes as described in Edwards et al., 2013 (**Figure 25**). This confirms the reliability of the inverted velocity profile in light of the current assumptions of one-dimensionality.

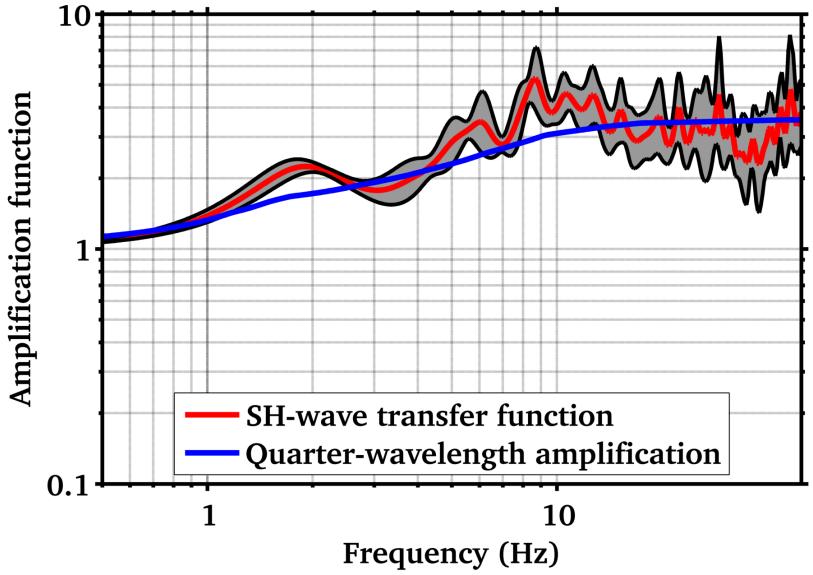

Figure 24 - *Comparison of amplification functions computed using the SH-wave transfer function and the quarter-wavelength formalism on the inverted velocity models. The functions are referenced to the Swiss rock reference model (Poggi et al. 2011).*

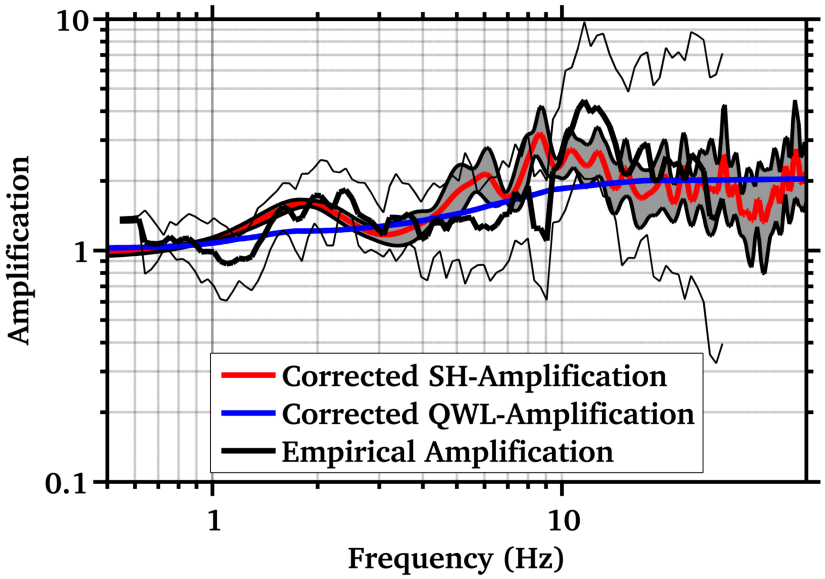

Figure 25 - *Comparison of amplification functions computed using the SH-wave transfer function and the quarter-wavelength approach with empirical observation from spectral modeling of low-magnitude earthquakes. All functions are referenced to the Swiss rock reference model (Poggi et al. 2011).*

REFERENCES

Capon, J., 1969. High resolution frequency wavenumber spectrum analysis, Proc. IEEE, 57, 1408-1418.

Burjanek, J., G. Stamm, V. Poggi, J.R. Moore, and D. Fäh [2010], "Ambient vibration analysis of an unstable mountain slope", Geophys. J. Int., Vol. 180, pp. 820-828.

Edwards, B., C. Michel, V. Poggi and D. Fäh (2013). Determination of Site Amplification from Regional Seismicity: Application to the Swiss National Seismic Networks. Accepted for publication in Seismological Research Letters.

Joyner, W. B., R. E. Warrick and T. E. Fumal (1981). The Effect of Quaternary Alluvium on Strong Ground Motion in the Coyote Lake, California, Earthquake of 1979, Bulletin of the Seismological Society of America, 71, 1333-1349.

Poggi, V., B. Edwards and D. Fäh (2011). Derivation of a Reference Shear-Wave Velocity Model from Empirical Site Amplification, Bulletin of the Seismological Society of America, 101, 258-274.

Poggi, V. and Fäh D., 2010. Estimating Rayleigh wave particle motion from three-component array analysis of ambient vibrations. Geophys. J. Int., 180-1, 251-267.